Numerical Heat Transfer, Part A: Applications: An International Journal of Computation and Methodology
Publication details, including instructions for authors and subscription information:
http://www.tandfonline.com/loi/unht20

Analysis of the Flow Agitated by Disc Impellers with Pitched Blades

Yeng-Yung Tsui [a] , Shih-Chao Lin [a] , Shih-Jhen Shen [a] & Yu-Chang Hu [a]
[a] Department of Mechanical Engineering , National Chiao Tung University , Hsinchu, Taiwan, Republic of China
Published online: 07 Jan 2008.

To cite this article: Yeng-Yung Tsui , Shih-Chao Lin , Shih-Jhen Shen & Yu-Chang Hu (2008) Analysis of the Flow Agitated by Disc Impellers with Pitched Blades, Numerical Heat Transfer, Part A: Applications: An International Journal of Computation and Methodology, 53:10, 1091-1108, DOI: 10.1080/10407780701790102

To link to this article: http://dx.doi.org/10.1080/10407780701790102

Numerical Heat Transfer, Part A, 53: 1091–1108, 2008

ISSN: 1040-7782 print/1521-0634 online
DOI: 10.1080/10407780701790102

Taylor & Francis
Taylor & Francis Group

ANALYSIS OF THE FLOW AGITATED BY DISC IMPELLERS WITH PITCHED BLADES

Yeng-Yung Tsui, Shih-Chao Lin, Shih-Jhen Shen, and Yu-Chang Hu

Department of Mechanical Engineering, National Chiao Tung University, Hsinchu, Taiwan, Republic of China

In this study we are concerned with the flow in a tank stirred by disc impellers with pitched blades. A mathematical method, based on multiframe of reference and unstructured grid technology, was employed in the flow simulation. It was learned from the study by Tsui et al. [12] that for a pitched-blade impeller, which does not include the disc, the flow pattern in the agitated tank is transformed from the axial type to the radial type at a particular angle when the blade angle is increased. A similar phenomenon was observed in the present study. However, in contrast to the results of Tsui et al., the change of flow pattern brings about a sharp decrease in power requirement and a jump in pumping capacity. The cause of the difference is related to the disc which obstructs the fluid when it flows in the axial direction at low blade angles and makes it flow smoothly in the radial direction along the disc at high blade angles. It was shown in the results that the transition angle is increased when the impeller size, the disc size as well as the off-bottom clearance are reduced.

INTRODUCTION

Fluid motion is essential for mixing processes required in various industries. To stir fluids a variety of agitators have been developed. When the working fluid is highly viscous, such as a large variety of non-Newtonian fluids, impellers with low speeds, but large in size, are frequently used. Helical ribbons and gate anchors are of this type. For low-viscosity fluids small impellers with a number of turbine blades are preferred because they can rotate at high speeds to produce high turbulence, which is helpful to fluid mixing. Among turbine blade impellers, pitched-blade turbines and Rrushton turbines are mostly widely employed.

The fluid flow generated by the pitched-blade turbine is classified as axial type because a single loop circulating from the top to the bottom dominates the flow field. For the Rushton turbine a stream emerging in radial direction from the periphery of the blades separates the flow field into two circulation loops. However,

Received 7 March 2007; accepted 22 October 2007.

This work was supported by the National Science Council of Taiwan, R.O.C., under contract number NSC-94-2212-E-009-024.

Address correspondence to Dr. Yeng-Yung Tsui, National Chiao Tung University, Department of Mechanical Engineering, 1001 Ta-Hsueh Road, Hsinchu 300, Taiwan, Republic of China. E-mail: yytsui@mail.nctu.edu.tw

NOMENCLATURE

B	baffle width	V_r, V_q, W	velocities in radial, circumferential, and axial directions
C	off-bottom clearance		
D	impeller diameter	V_{tip}	blade tip velocity
D	disc diameter	W	blade width
D_s	shaft diameter	x_j	Cartesian coordinates of the considered point
F^c	convection flux		
F^d	diffusion flux	Z	vertical distance
H	tank height	α	pitch angle
k	turbulent kinetic energy	$\vec{\delta}_{PC}$	distance vector directed from P to C
N	rotational speed		
N_P	power number	ε	turbulent dissipation rate
N_Q	pumping number	ε_{ijk}	alternating unit tensor
Q	net mass flux through all blade passages	ϕ	a flow property
		γ	blending factor
$\vec{r}$	position vector relative to the rotation axis	Γ_ϕ	diffusion coefficient for ϕ
		η	pumping efficiency
$\vec{s}_f$	surface vector	τ	torque
S_ϕ	source term of transport equation for ϕ	$\vec{\Omega}$, Ω_m	angular speed
		Subscripts	
T	tank diameter	f	face value
$\vec{U}_g$, U_{gj}	grid velocity vector	ϕ	for the flow property ϕ
U_j	flow velocity vector		

the flow patterns may be changed by the settings of the impeller system. The velocity measurements for a 60° pitched-blade impeller conducted by Nouri and Whitelaw [1] revealed that the flow pattern shifts from the axial to the radial type when the Reynolds number becomes smaller than a value around 650. This flow transition was confirmed by the power measurements of Hockey and Nouri [2] in which the power number increases sharply at $\text{Re} = 1200$ as Reynolds number is increased. The mixing systems used in both studies were geometrically similar, but the size of the former was half of the latter. This implies direct proportionality of the critical Reynolds number to the system size. The change of flow pattern from axial to radial type was also visualized at Reynolds numbers $490 \sim 500$ in the experiments by Schafer et al. [3]. It is noted that the Reynolds numbers at which the flow transition occurs are in the laminar regime, whereas this kind of impeller usually operates in the turbulent regime.

The clearance between the impeller and the bottom of the vessel is another parameter affecting the flow structure. For a pitched-blade turbine with diameter $D = T/3$ the experimental study of Jaworski et al. [4] showed that when the off-bottom clearance changes from $T/4$ to $T/2$, the strength of the dominant circulation loop decreases and a secondary circulation loop rotating in the opposite direction of the main one forms in the bottom region. A similar observation was reported by Mao et al. [5] that with a $D = T/2$ pitched-blade turbine located at clearance $C = T/2$ a secondary loop is clearly visible in the bottom region. However, as the clearance or the impeller is reduced to $T/3$ only one circulation loop prevails. Similar results can also been seen in the work done by Kresta and Wood [6]. For an extreme case with $D = 3T/5$ and $C = T/2$ in the study of Mao et al. the stream is discharged

from the blade passage in nearly radial direction and the secondary loop occupies almost the entire lower part of the vessel.

Yianneskis et al. [7] reported that with a Rushton turbine impeller the inclination of the impeller stream increases with decreasing clearance. Rutherford et al. [8] investigated the flow in a vessel stirred by two Rushton Impellers. They reported that the flow pattern depends strongly upon the off-bottom clearance of the lower impeller, the separation between the two impellers, and the submergence of the upper impeller below the top. Three stable flow patterns, termed parallel flow, merging flow and diverging flow, were identified according to the choices of the three parameters. The diverging flow was observed as the clearance becomes smaller than $0.15T$. In this flow the discharge stream emerging from the lower impeller is directed towards the base of the vessel when it moves out of the circular disc of the Rushton impeller. The above flow patterns were also evidenced in the numerical computations by Micale et al. [9] and Deshpande and Ranade [10]. The direction of the impeller stream towards the bottom of the vessel for $C < 0.15T$ was confirmed in the experiments with a single Rushton turbine impeller by Montante et al. [11]. It was shown by their measurements that the flow angle of the stream is around 25° to 30° to the horizontal for $C = 0.2\,T$, indicating that the flow field becomes partly axial at this clearance. Further reduction of the clearance leads to the transition to fully axial type flow.

A recent study conducted by Tsui et al. [12] using numerical method systematically examined the effect of blade angle on the flow in a vessel stirred by the pitched-blade turbine impeller. It was shown that the flow pattern is transformed from the axial type to the radial type when the blade angle is beyond a certain value. For the impeller with a diameter $D = T/3$ this critical angle increases from 50° to 76° and 87° as the clearance decreases from $C = T/2$ to $C = T/3$ and $T/4$, respectively. When the impeller diameter is enlarged to $D = T/2$, the corresponding critical angles are reduced to 40°, 70°, and 87°. The change of flow pattern to radial type causes a jump in power requirement, along with a sharp decline in pumping flow rate and, thus, the pumping efficiency.

The Rushton turbine impeller includes a circular disc with a number of flat blades mounted vertically around its periphery. It produces strong circulating flow at the cost of large power consumption. To relieve the high power requirement the flat blades can be installed in a pitched manner, i.e., skew to the disc. As a consequence, the flow is complicated because the disc tries to make the discharge stream flow in the radial direction while the pitched blades tend to form axial flow. The combined effect of the pitched blade and the disc becomes the main concern of the present study. In the following, the mathematical method used to analyze the flow is briefly described first. Then, the computed results are discussed for different setups of the impeller system.

MATHEMATICAL METHOD

The flow agitated by high-speed impellers is inevitably unsteady, three dimensional, and turbulent. To deal with this unsteady flow either the LES (large eddy simulation) or the ensemble-averaged turbulence models can be chosen. In LES, not only the mean flow, but also a range of large scales of motion is directly calculated.

Therefore, it is appealing for stirring flow simulations [13, 14]. Very fine grids are required in LES to allow simple turbulence modeling at the subgrid scale and a sufficiently long time is needed to extract meaningful statistics. Besides, the full flow field needs to be modeled without taking advantage of symmetric or periodic conditions. As an example, the simulation of Derksen and Van den Akker [13], incorporating a grid with 180^3 cells and making a run of 60 impeller revolutions, require almost a month to complete computation on a HP-Convex S-class parallel computer with four processing units and 1 Gbyte memory.

In order to reduce computational effort, a way is to assume that the flow is in the quasi-steady state, in which the relative motion of the impeller to the rest of the vessel is frozen. In steady-state calculations the ensemble-averaged turbulence models must be used. It was reported by Wechsler et al. [15] that with the use of the standard k-ε model the steady-state approach can yield results in good agreement with fully unsteady computations, but only at a fraction of time and expense. In principle, Reynolds stress models are more fundamental and universal than eddy-viscosity models. However, they still require more elaborate modelings. Comparing with the eddy-viscosity models, more effort is needed for Reynolds stress models because seven additional transport equations need to be solved and it is difficult for the solution iteration to reach convergence. It was reported by Bakker et al. [16] and Sheng et al. [17] that there is very little difference in the mean flow sirred by a 45° pitched-blade turbine between the predictions using the Reynolds stress model, the RNG k-ε model and the standard k-ε model. Greater differences are found only in turbulence properties. In the category of eddy-viscosity model two-equation models are most widely adopted. In the study of Jenne and Reuss [18] three different k-ε models were assessed while six two-equation models, including three k-ε versions and three k-ω versions, were compared by Jones et al. [19]. All these models obtained overall quantitave agreement with measurements, except in the impeller discharge region. No particualr models are much superior to the others. Therefore, the standard k-ε model is emplyed in the following computations.

In the steady-state calculations the impeller blades are fixed at a specific position. To trigger fluid flow, several means have been developed. In the momentum source boundary condition method of Xu and McGrath [20] the impeller blade is divided into a number of strips and each strip is regarded as an airfoil. The lift and drag forces produced on the airfoil are added to the momentum equations as boundary sources to drive the flow. In the snapshot method [21, 22] the interaction between the fluid and the impeller is modeled via implementation of mass and momentum sources/sinks at the computational cells adjacent to the impeller blades. These sources/sinks are used to characterize the effect of the blade movement. A more popular method makes use of the concept of multiframe of [23, 24]. The stirred vessel is divided into two regions. In the inner region, encompassing the impeller, the reference frame rotates with the impeller while the rest part is stationary. It is noted that the computational mesh in the rotational region is fixed without motion. The governing equations for conservation of mass and transported properties can be cast into the following forms.

$$\frac{\partial}{\partial x_j}[\rho(U_j - U_{gj})] = 0 \tag{1}$$

$$\frac{\partial}{\partial x_j}[\rho(U_j - U_{gj})\phi] = \frac{\partial}{\partial x_j}\left(\Gamma_\phi \frac{\partial \phi}{\partial x_j}\right) + S_\phi \tag{2}$$

where ρ is the fluid density, ϕ the transport variable, and Γ_ϕ the diffusivity. In the equation U_j is the Cartesian velocity component and U_{gj} the grid velocity component defined by

$$\vec{U}_g = \vec{\Omega} \times \vec{r} \text{ in the rotational region} \tag{3a}$$

$$\vec{U}_g = 0 \text{ in the stationary region} \tag{3b}$$

where $\vec{\Omega}$ is the angular velocity vector of the impeller and $\vec{r}$ the position vector relative to the rotation axis. In this study the standard k-ε model is adopted to characterize turbulence. The transport property ϕ represents $U_j - U_{gj}$, k, and ε. The correspondung source term for the momentumn equation is given by

$$S_{U_j} = -\frac{\partial p}{\partial x_j} - \rho\varepsilon_{mnj}\Omega_m(\varepsilon_{pqn}\Omega_p x_q) + 2\rho\varepsilon_{mnj}\Omega_m(U_n - U_{gn}) \tag{4}$$

It is noted in the expression that the two terms other than the pressure gradient stand for the centrifugal force and the Corriolis force, respectively, produced by the rotation of the impeller, which must be dropped in the stationary region. In these terms the symbol ε_{ijk} is the alternating unit tensor.

Discretization of the governing equations is based on a fully conservative finite volume method applicable to unstructured grids which can be made of control volumes with arbitrary polyhedron geometry. First, the differential equations, being of divergence form as shown above, are integrated over a control volume. By applying the divergence theorem the volume integrals of the convection and diffusion terms are transformed into surface integrals. The convection flux though the surface of the control volume is given as

$$F^c = \sum_f (\rho(\vec{U} - \vec{U}_g)\vec{s})_f \phi_f \tag{5}$$

Here the subscripts f denote a face on the control volume, $\vec{s}_f$ is the surface vector of the considered face as shown in Figure 1, and the summation is taken over all the faces of the control volume. The face value ϕ_f is approximated by a second-order upwind differencing,

$$\phi_f = \phi^{UD} + \gamma(\nabla\phi)^{UD}\vec{\delta} \tag{6}$$

where the superscripts UD denote the value evaluated at the node upwind of the considered face, $\vec{\delta}$ is a vector directed from the upwind node to the centroid of the face. The blending factor γ is a value between 0 and 1. For $\gamma = 0$ it is the well-known upwind difference scheme while for $\gamma = 1$ a second-order scheme. The diffusion flux is estimated by a second-order approximation

$$F^d = \sum_f \left[\frac{\Gamma_f s_f^2}{\vec{\delta}_{PC}\vec{s}_f}(\phi_C - \phi_P) + \Gamma_f \overline{\nabla\phi}_f \left(\vec{s}_f - \frac{s_f^2}{\vec{\delta}_{PC}\vec{s}_f}\vec{\delta}_{PC}\right)\right] \tag{7}$$

where, see Figure 1, the subscripts P denote the principal node and the subscripts C a neighboring node, $\vec{\delta}_{PC}$ is a vector connecting these two nodes. The face gradient $\overline{\nabla\phi}_f$

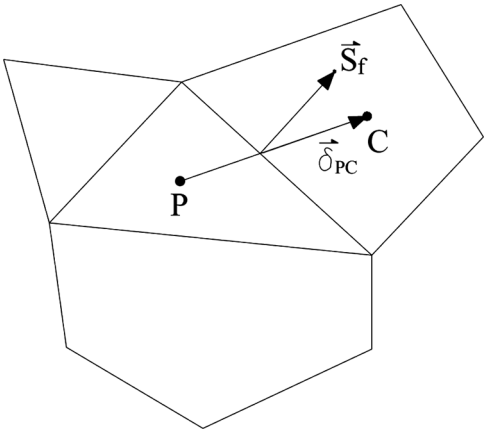

Figure 1. Illustration of a control volume.

is obtained via interpolation from the gradients at the two adjacent nodes P and C. The deferred correction procedure is used to treat the two terms in the convection and diffusion fluxes. That is, the first terms on the right hand side in the above Eqs. (6) and (7) are handled in an implicit way to construct the coefficients of the resulted difference equation whereas the second terms are treated explicitly and absorbed into the source term.

As the SIMPLE algorithm, a pressure-correction equation is derived by forcing the predicted velocities, obtained after solving the discretized momentum equations, to satisfy the continuity constraint. The linearized difference equations for the velocity components, the pressure correction, and other variables are solved sequentially in a segregated manner. Outer iterations are performed to take into account the non-linearities, the coupling between the variables, and those terms treated explicitly mentioned above. More details about this method can be found in [25, 26].

RESULTS AND DISCUSSION

A sketch of the considered stirring system is shown in Figure 2. The system is composed of a 4-baffled tank and a disc turbine with six pitched blades. The tank has a diameter $T = 300\,\text{mm}$ with its height $H = T$. The influence of the impeller size as well as the disc size had been examined. Three different impellers were under investigation. Two of them are of the same impeller diameter ($D = T/3$) but different in disc diameter ($d = 2D/3$ and $3D/4$). The third one has a larger impeller diameter $D = T/2$ and a larger disc diameter $d = 3D/4$. The off-bottom clearance C changes from $T/2$ to $T/3$ and further to $T/4$. The blades have a constant width $W = T/10$, but vary in length in accordance with the impeller diameter ($L = D/4$). The pitch angle of blade α is allowed to vary between 30° and 90°. For $\alpha = 90^\circ$ the blades are in vertical position and the impeller becomes a Rushton turbine. The width of baffle is fixed at $B = T/10$. The impeller rotates at a speed of 5 rps. Due to the symmetric arrangement of the blades and the baffles shown in Figure 2, the flow in the tank is periodic for a circumferential span of 180°. Hence, only half a tank

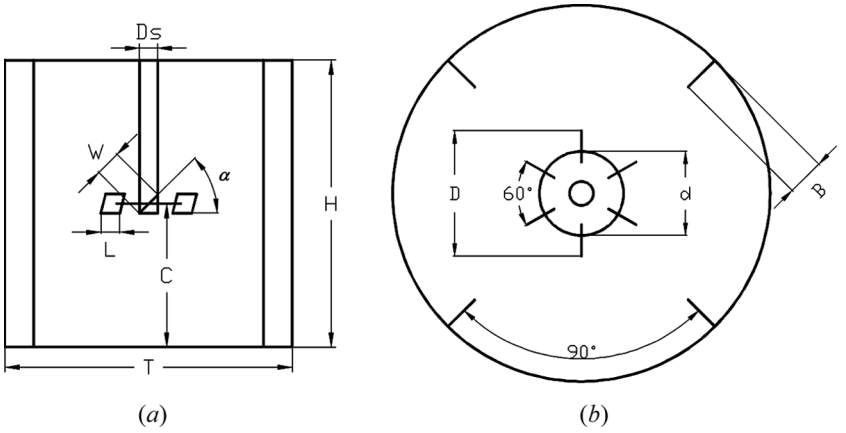

Figure 2. A sketch of the stirred tank.

was considered as the computational domain in calculations. A typical grid layout is shown in Figure 3.

To validate the methodology and assess grid sensitivity Figure 4 is prepared. Meshes with four different grid densities had been tested and comparison was made with the experiments of Ranade and Joshi [27] in which a Rushton turbine was under investigation. The configurations of the agitating system are $D = T/3$, $d = 2D/3$, and $C = T/2$. The velocities in the axial (W), radial (V_r), and circumferential (V_q) directions at locations $2Z/H = 0.2$ and 0.933 below the disc are exhibited. It is obvious from the figure that in general, the predictions can well reflect the basic

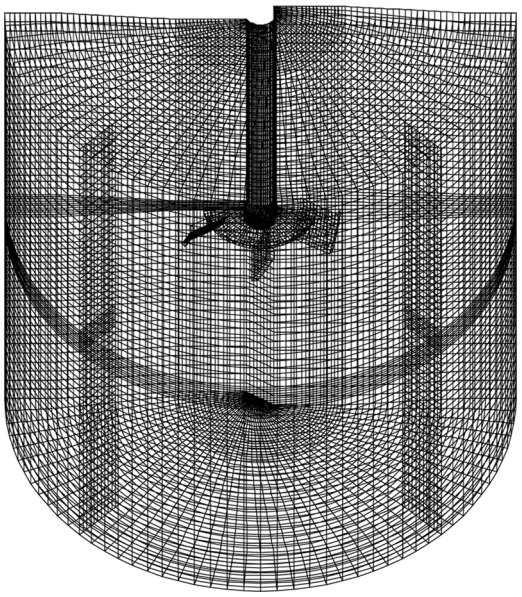

Figure 3. A typical grid.

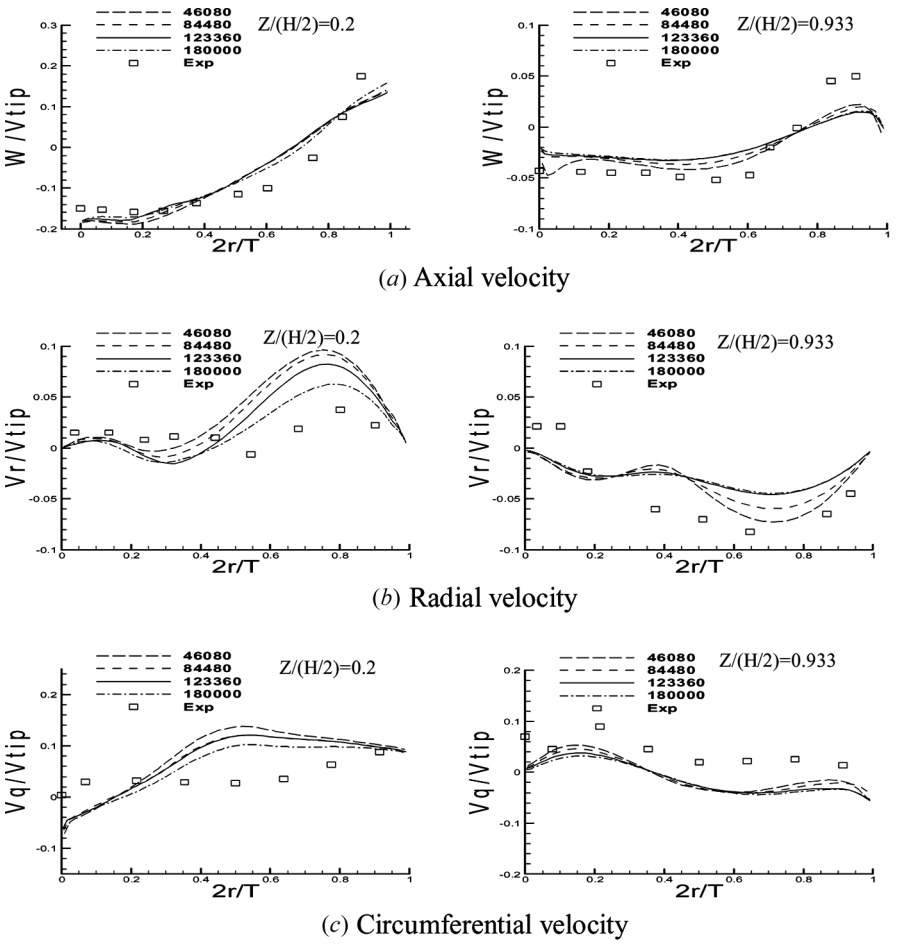

Figure 4. Comparison of predictions with measurements.

physics of the fluid flow. With finer meshes better agreement with measurements is obtained. A list of the predicted power numbers and pumping numbers are given in Table 1. It is generally accepted that the power number for a Rushton turbine is around a value of 5. Evidently, the predicted values agree well with the data of Ranade and Joshi and are quite close to each other except for the coarsest mesh. In the following, the results using a mesh with about 120,000 cells are reported.

Table 1. Comparison of predicted power numbers and pumping numbers for different grids

Predictions					
Grid	46,080	84,480	123,360	180,000	Exp. [27]
N_P	4.93	5.03	5.04	5.05	4.9
N_Q	0.81	0.83	0.84	0.85	0.75

The power number is defined by

$$N_p = \frac{P}{\rho N^3 D^5} = \frac{2\pi\tau}{\rho N^2 D^5} \tag{8}$$

where $P = 2\pi N\tau$ stands for the power requirement and N the rotational speed. The torque τ is done by the pressure force as well as the frictional force. The pressure force is resulted from the pressure difference between the two surfaces of the blade. The frictional force is exerted on the circular disc, the blade surfaces, and the shaft surface. The part of torque produced by the frictional force is usually much smaller than that by the pressure force and may be negligible. However, it becomes more significant at small pitch angles of blade.

Loop circulation is a main feature of the flow in the stirred tank and is responsible for the fluid mixing. Its strength depends on the discharge flow pumped by the impeller. Thus, the pumping number is defined as

$$N_Q = \frac{Q}{\rho N D^3} \tag{9}$$

where Q is the net mass flux through the impeller, which is obtained via integrating over the surface surrounding the volume swept by the blades.

Effects on Flow Pattern

To illustrate the effect of the blade angle on the flow pattern the streamlines on a vertical plane in the middle between two adjacent blades for a case with $D = T/3$, $d = 3D/4$, and $C = T/3$ are shown in Figure 5. For blade angles between 66° and 90° the flow is of radial type with a circulation loop occupying either side of the impeller. As the angle is reduced to less than 65°, the impeller stream makes a sudden change of flow direction towards the bottom at the edge of the disc. Thus, the flow becomes an axial type with a large circulation loop dominating the flow field and a much small one being restricted in the region beneath the impeller. This phenomenon is similar to that for a pitched-blade turbine without the circular disc reported by Tsui et al. [12].

For better understanding of the flow pattern the flow angle of the discharge stream is under examination. As shown in Figure 6, the flow angle β is defined as the orientation of the line connecting the tip of the disc and the point on the wall separating the two circulation loops. The flow angles for all considered cases are presented in Figure 7. The flow angle is around 80° at blade angle $\alpha = 30°$. It decreases slowly with increasing blade angle in a nearly linear fashion. At the blade angle where the flow pattern changes the flow angle β drops sharply by a value of about 60°. It follows by a slow decrease to 0° at $\alpha = 90°$. A summary of the critical angles at which the transition takes place is given in Table 2. It is seen that the off-bottom clearance has a definite impact on the flow pattern. At $C = T/2$ the double circulation loop pattern prevails for a wide range of blade angles. As the clearance decreases to $T/4$, the transition occurs at a high angle close to 90° for $D = T/3$. It is prone for the flow to become single loop pattern for small clearances, which was evidenced in references 4–6 for the pitched-blade turbine impeller and in [11] for the Rushton turbine impeller. It can also be seen from the table that the critical angle is decreased when the disc is enlarged from $2D/3$ to $3D/4$. This is expected

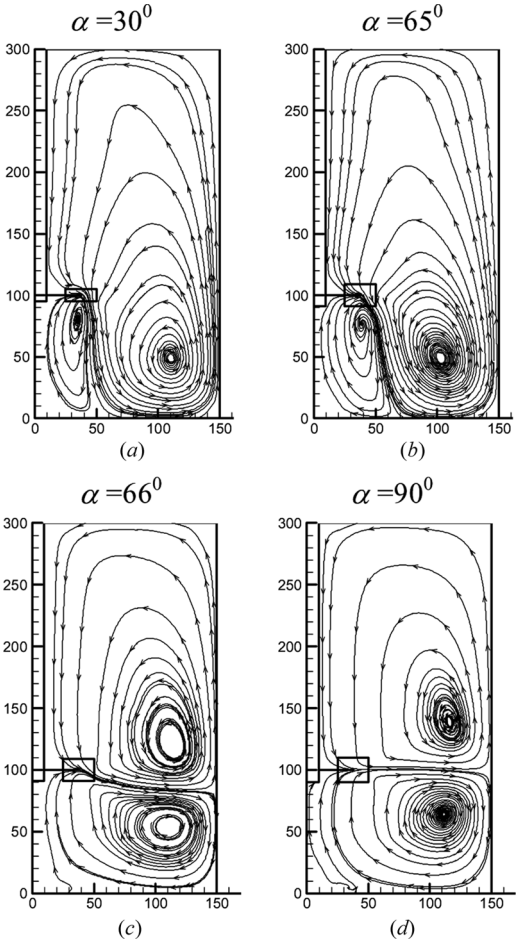

Figure 5. Flow streamlines for the impeller with $D = T/3$ and $d = 3d/4$ at $C = T/3$.

because the disc shapes the flow in the radial direction and makes it friendlier to the radial type flow. The transition angle can be further reduced by enlarging the impeller size. For the extreme case with $D = T/2$, $d = 3D/4$, and $C = T/2$ the flow remains as radial type for all blade angles under consideration.

Effects on Power Requirement

The dependence of power number on blade angle for the cases considered is illustrated in Figure 8. Generally, the power consumption increases with the blade angle due to the fact that both the blade area projected on the vertical plane and the pressure difference between the two side surfaces of the blade increases as the flat blade approaches the vertical position. The sudden change from the axial type to the radial type results in sharp reduction of power number. This is especially true for the cases with $d = 3D/4$. The extent of reduction becomes more prominent when

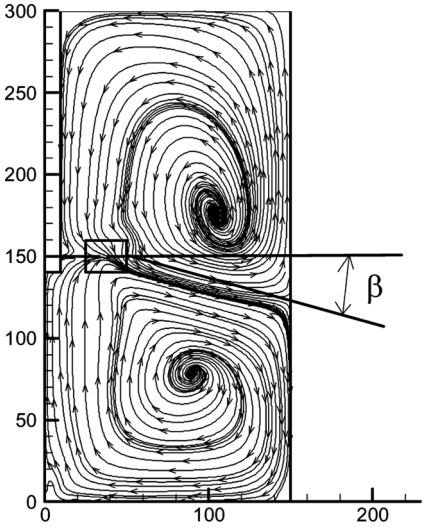

Figure 6. Define flow angle of the discharge stream.

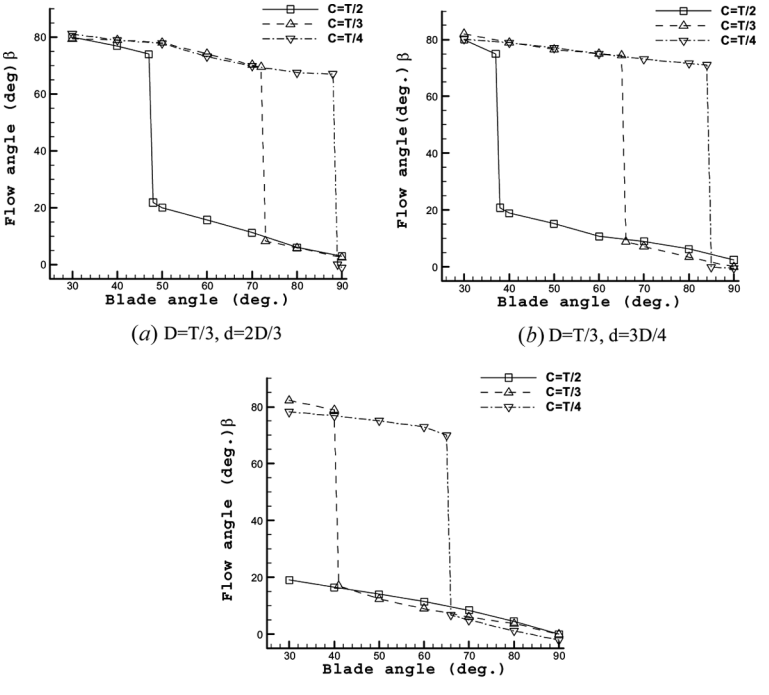

Figure 7. Variation of the flow angle against the pitch angle of the blade.

Table 2. A summary of transition blade angles

	$C = T/2$	$C = T/3$	$C = T/4$
$D = T/3$, $d = 2D/3$	47°	72°	88°
$D = T/3$, $d = 3D/4$	37°	65°	84°
$D = T/2$, $d = 3D/4$	—	40°	65°

the clearance is small and no appreciable change is detected for $C = T/2$. For the impeller with $D = T/3$ and $d = 2D/3$ the effect of clearance on the power number is not as significant as the other impellers. It is interesting to notice that with this impeller the power number, contrary to the others, increases slightly instead of decreases at the critical angle for $C = T/2$.

The result of sharp decline in power requirement at the transition point is in contrast to that reported in [12]. This difference is related to the existence of the disc. Without the disc the flow induced can pass the passage between the blades freely without any hindrance. With the disc the flow is forced to move along the disc first, followed by a sharp turn for the axial type flow as seen in Figure 5. For the radial type the flow sweeps across the disc and moves smoothly out of the blade passage.

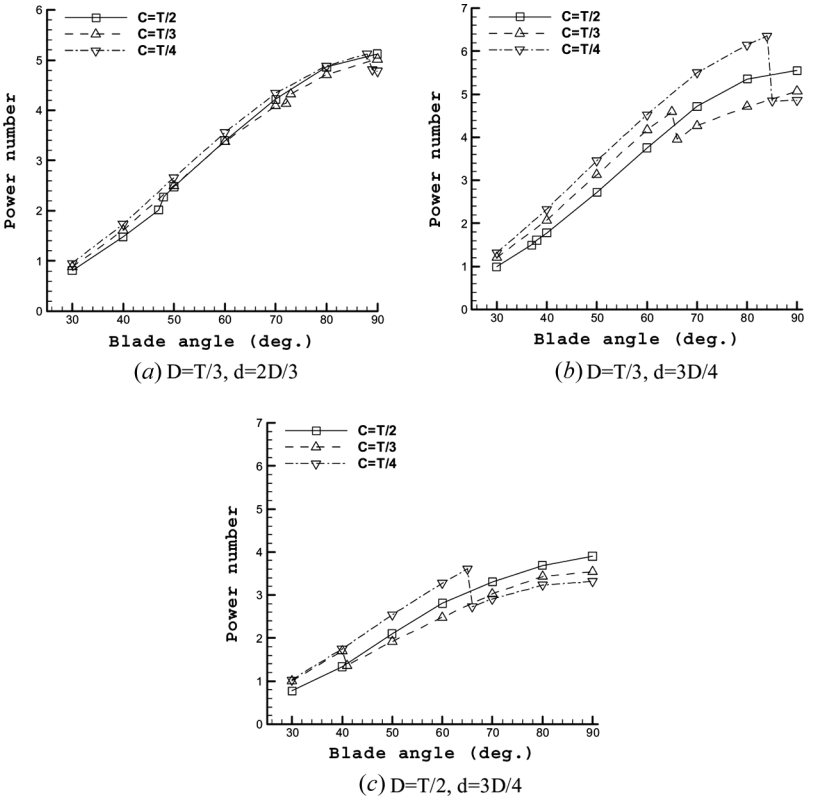

Figure 8. Variation of the power number against the pitch angle of the blade.

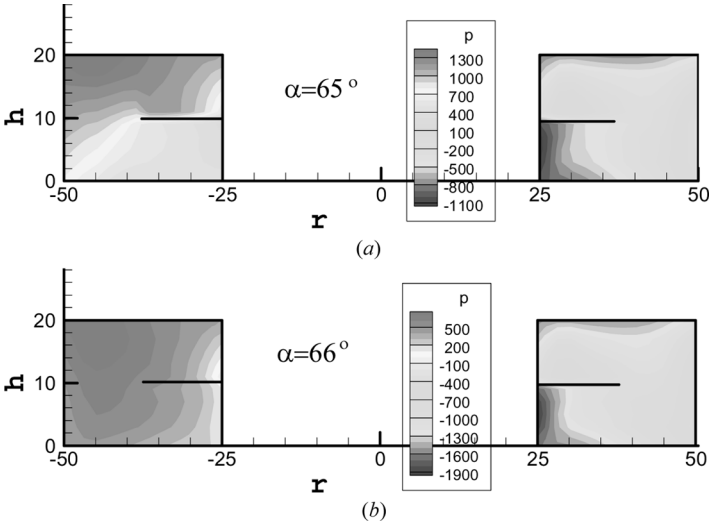

Figure 9. Pressure contours on the surface of a blade for $\alpha = 65^\circ$ and 66° for the case with $D = T/3$, $d = 3D/4$, and $C = T/3$. The sketches on the left are referred to the front surface and those on the right to the back surface.

Such a change of flow pattern is related to the pressure field. A close look of the pressure distribution on the two surfaces of a blade for the two flow types is shown in Figure 9. The plots on the left are referred to the front surface while those on the right to the back surface. The pressure on the front surface is high in the upper half, especially in the region near the outer edge, for the blade angle $\alpha = 65^\circ$. This high pressure forces fluid to flow downward to form axial flow. For $\alpha = 66^\circ$ the pressure distribution is more uniform and more symmetrical to the disc. Thus, the flow is of radial type. The pressure level on the back surface is much lower than that on the front surface, with a minimum at the inner edge region beneath the disc. The mean pressure difference between the two surfaces is lower for $\alpha = 66^\circ$, leading to a decrease in the power requirement. To further illustrate the effects of pressure on the flow field, the pressure distribution in a vertical plane for the entire vessel is given in Figure 10. An obvious difference between the two flow types is that for $\alpha = 65^\circ$ a very low pressure zone is formed in the center region beneath the disc while for $\alpha = 66^\circ$ a low pressure zone, being much smaller and weaker, appears at the outer edge of the turbine blade. In the former the pressure gradients are much greater than those in the latter. Thus, it can be concluded that it is the pressure gradient driving the flow to change from the axial type to the radial type when the blade angle becomes greater than the critical angle.

Effects on Pumping Capacity

The variation of the pumping number, defined by Eq. (9), against the pitch angle of the blade is shown in Figure 11. The pumping number, in general, increases with the blade angle and makes a jump at the transition angle. The effect of clearance

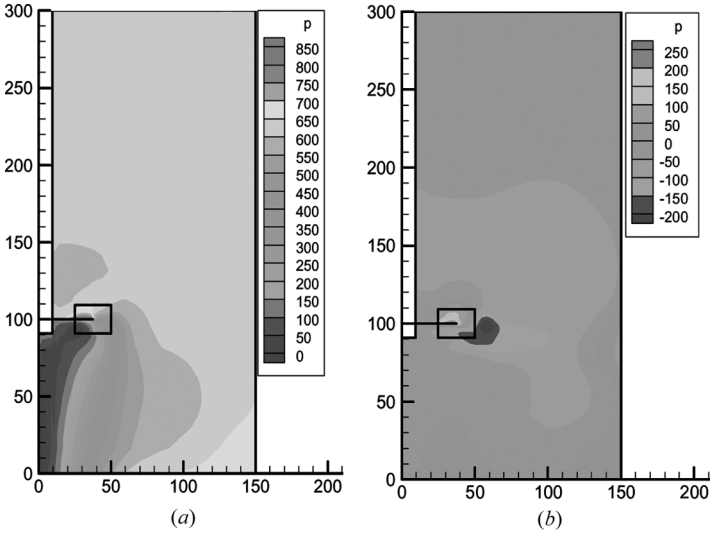

Figure 10. Pressure distribution in a vertical plane for $\alpha = 65^{\circ}$ and 66° for the case with $D = T/3$, $d = 3D/4$, and $C = T/3$.

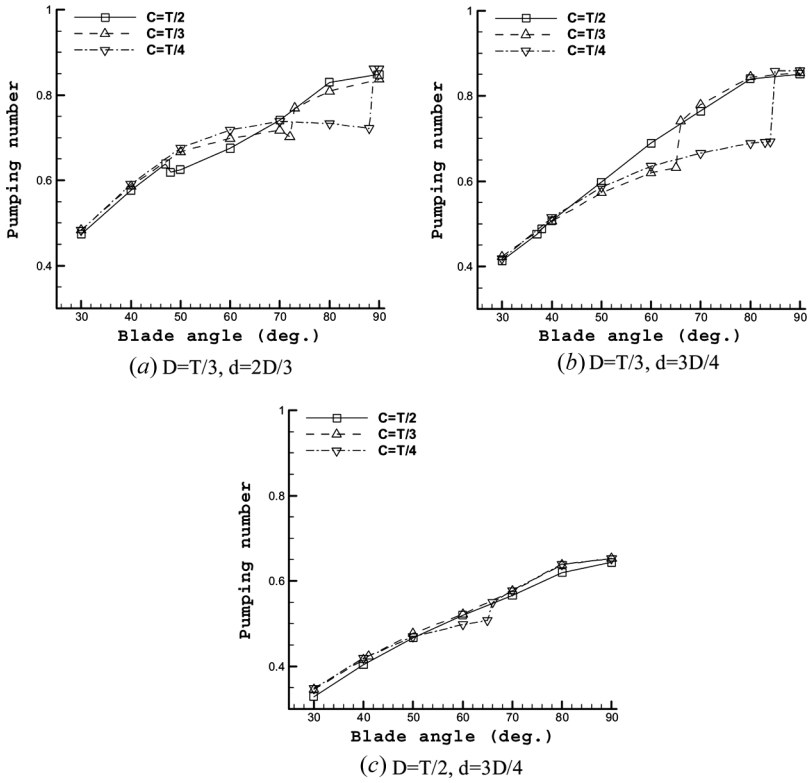

Figure 11. Variation of the pumping number against the pitch angle of the blade.

is not significant for the impeller with $D = T/2$ and for those cases with $D = T/3$ at small blade angles. Different from the others, in the cases with $D = T/3$ and $d = 2D/3$ the pumping number levels off and tends to decline before reaching the critical angle for $C = T/3$ and $T/4$. For $C = T/2$ the pumping number decreases instead of increases at the transition blade angle. To look into inside of the flow through the blade passage, the flow is separated into four parts related to the four edges of the blade. The pumping numbers corresponding to these four flows, together with the net flow pumping number for the case with $D = T/3$, $d = 3D/4$, and $C = T/3$, are shown in Figure 12. It is seen that the flow through the upper edge and the inner edge of the turbine blade varies smoothly with the blade angle. The flow through the lower edge increases slightly first. It is followed by a slight decrease until the critical angle is reached. A sharp decline takes place at this transition angle, followed by a gradual decrease. The flow through the outer edge varies in an opposite manner to the lower edge flow.

Effect on Pumping Effectiveness

The effectiveness of the pumping activity done by the impeller is represented by the pumping efficiency given by

$$\eta = \frac{N_Q}{N_P} \tag{10}$$

It stands for the pumping capability for a unit of power input. In contrast to the pumping number, the pumping efficiency decreases with increasing blade angle, as shown in Figure 13. The curves level off when the blade angle approaches 90°. At the transition angle, a jump is easily detected except for those cases with $C = T/2$.

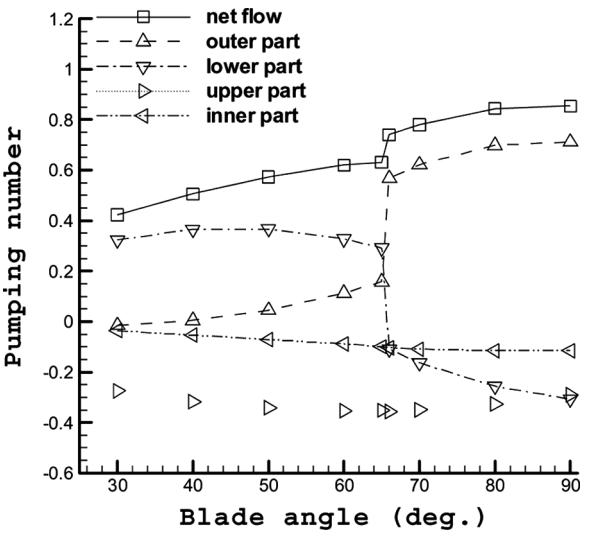

Figure 12. Variation of pumping numbers for different parts of the blade passage against the pitch angle of the blade.

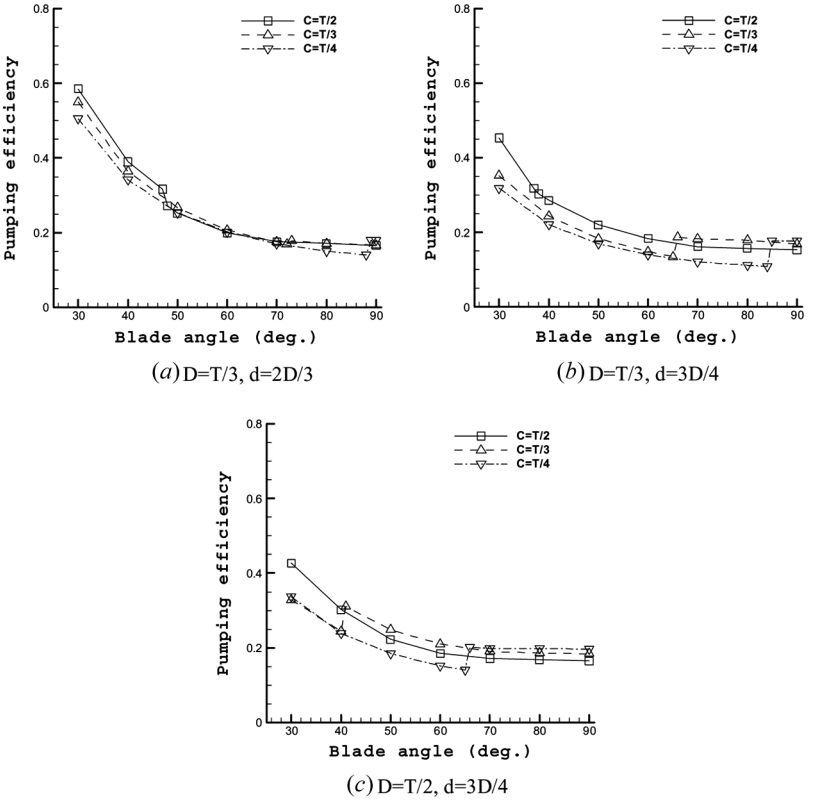

Figure 13. Variation of the pumping efficiency against the pitch angle of the blade.

For the case with $D = T/3$, $d = 2D/3$, and $C = T/2$ the efficiency has a sharp decrease at the transition angle, which is not unexpected in view of the variation of N_Q and N_P seen in the above. The impeller with $D = T/3$ and $d = 2D/3$ has higher efficiency than the other two impellers, especially for small blade angles.

CONCLUSIONS

The flow in a vessel stirred by disc impellers with pitched blades has been investigated by a numerical means. The mathematical model is based on a quasi-steady state assumption and the use of multiframe of reference to deal with the rotation of the impeller. Discretization of the governing equations is fulfilled by a finite volume method suitable for the use of unstructured grid technology. The main findings are summarized in the following.

1. By varying the pitch angle of the blade there exists a critical angle, above which the flow pattern is of radial type with two circulation loops separated by the impeller, and below which the flow is of axial type with a main circulating loop dominating the entire tank apart from the region just beneath the disc where a secondary looping flow forms.

2. The cause of the change of flow type is due to the dramatic change of the pressure distribution in the vessel when the blade angle exceeds the critical value. In the axial type of flow a very low pressure zone is formed beneath the circular disc whereas low pressures appear at the outer edge of the blade turbine for the radial type of flow.
3. As the blade angle increases, the power number and pumping number increase, but the pumping efficiency decreases, except at the transition angle.
4. At the transition blade angle where the flow pattern changes from the axial type to the radial type, the power requirement is reduced while the pumping capability and efficiency are increased except for the impeller with $D = T/3$ and $d = 2D/3$ placed at $C = T/2$. This result is contradictory to that for a pitched-blade impeller without disc. The cause of the difference can be understood in viewing that the flow is obstructed by the disc in the axial type flow and, thus, needs to make a sharp turn at the edge of the disc.
5. The impeller size, the disc size together with the off-bottom clearance all have a great influence on the transition angle. This angle is reduced when the values of these parameters are increased.

REFERENCES

1. J. M. Nouri and J. H. Whitelaw, Flow Characteristics of Stirred Reactors with Newtonian and Non-Newtonian Fluids, *AIChE J.*, vol. 36, pp. 627–629, 1990.
2. R. M. Hockey and J. M. Nouri, Turbulent Flow in a Baffled Vessel Stirred by a 60° Pitched Blade Impeller, *Chem. Eng. Sci.*, vol. 51, pp. 4405–4421, 1996.
3. M. Schafer, M. Yianneskis, P. Wachter, and F. Durst, Trailing Vortices around a 45° Pitched-Blade Impeller, *AIChE J.*, vol. 44, pp. 1233–1246, 1998.
4. Z. Jaworski, A. W. Nienow, E. Koutsakos, K. Dyster, and W. Bujalski, An LDA Study of Turbulent Flow in a Baffled Vessel Agitated by a Pitched Blade Turbine, *Trans. IChemE. A*, vol. 69, pp. 313–320, 1991.
5. D.-M. Mao, L.-F. Feng, K. Wang, and Y.-L. Li, The Mean Flow Field Generated by a Pitched Blade Turbine: Changes in the Circulation Pattern due to Impeller Geometry, *Can. J. Chem. Eng.*, vol. 75, pp. 307–316, 1997.
6. S. M. Kresta and P. E. Wood, The Mean Flow Field Produced by a 45° Pitched Blade Turbine: Changes in the Circulation Pattern due to Off Bottom Clearance, *Can. J. Chem. Eng.*, vol. 71, pp. 42–53, 1993.
7. M. Yianneskis, Z. Popiolek, and J. H. Whitelaw, An Experimental Study of the Steady and Unsteady Flow Characteristics of Stirred Reactors, *J. Fluid Mech.*, vol. 175, pp. 537–555, 1987.
8. K. Rutherford, K. C. Lee, S. M. S. Mahmoudi, and M. Yianneskis, Hydrodynamic Characteristics of Dual Rushton Impeller Stirred Vessels, *AIChE J.*, vol. 42, pp. 332–346, 1996.
9. G. Micale, A. Brucato, F. Grisafi, and M. Ciofalo, Prediction of Flow Fields in a Dual-Impeller Stirred Vessel, *AIChE J.*, vol. 45, pp. 445–464, 1999.
10. V. R. Deshpande and V. V. Ranade, Simulation of Flows in Stirred Vessels Agitated by Dual Rushton Impellers Using Computational Snapshot Approach, *Chem. Eng. Comm.*, vol. 190, pp. 236–253, 2003.
11. G. Montante, K. C. Lee, A. Brucato, and M. Yianneskis, An Experimental Study of Double-to-Single-Loop Transition in Stirred Vessels, *Can. J. Chem. Eng.*, vol. 77, pp. 649–659, 1999.

12. Y.-Y. Tsui, J.-R. Chou, and Y.-C. Hu, Blade Angle Effect on the Flow in a Tank Agitated by the Pitched-Blade Turbine, *ASME J. Fluids Eng.*, vol. 128, pp. 774–782, 2006.
13. J. Derksen and H. E. A. Van den Akker, Large Eddy Simulations on the Flow Driven by a Rushton Turbine, *AIChE J.*, vol. 45, pp. 209–221, 1999.
14. H. S. Yoon, S. Balachandar, M. Y. Ha, and K. Kar, Large Eddy Simulation of Flow in a Stirred Tank, *ASME J. Fluids Eng.*, vol. 125, pp. 486–499, 2003.
15. K. Wechsler, M. Breuer, and F. Durst, Steady and Unsteady Computations of Turbulent Flows Induced by a 4/45° Pitched-Blade Impeller, *ASME J. Fluids Eng.*, vol. 121, pp. 318–329, 1999.
16. A. Bakker, K. J. Myers, R. W. Ward, and C. K. Lee, The Laminar and Turbulent Flow Pattern of a Pitched Blade Turbine, *Trans. IChemE. A*, vol. 74, pp. 485–491, 1996.
17. J. Sheng, H. Meng, and R. O. Fox, Validation of CFD Simulations of a Stirred Tank Using Particle Image Velocimetry Data, *Can. J. Chem. Eng.*, vol. 76, pp. 611–625, 1998.
18. M. Jenne and M. Reuss, A Critical Assessment on the Use of k-ε Turbulence Models for Simulation of the Turbulent Liquid Flow Influenced by a Rushton-Turbine in Baffled Stirred-Tank Reactors, *Chem. Eng. Sci.*, vol. 54, pp. 3921–3941, 1999.
19. R. M. Jones, A. D. Harvey III, and S. Acharya, Two-Equation Turbulence Modeling for Impeller Stirred Tanks, *ASME J. Fluids Eng.*, vol. 23, pp. 640–648, 2001.
20. Y. Xu and G. McGrath, CFD Predictions of Stirred Tank Flows, *Trans. IChemE. A*, vol. 74, pp. 471–475, 1996.
21. V. V. Ranade and S. M. S. Dommeti, Computational Snapshot of Flow Generated by Axial Impellers in Baffled Stirred Vessels, *Trans. IChemE. A*, vol. 74, pp. 476–484, 1996.
22. V. V. Ranade, An Efficient Computational Model for Simulating Flow in Stirred Vessels: a Case of Rushton Turbine, *Chem. Eng. Sci.*, vol. 54, pp. 4473–4484, 1997.
23. A. D. Harvey III, C. K. Lee, and S. E. Rogers, Steady-State Modeling and Experimental Measurement of a Baffled Impeller Stirred Tank, *AIChE J.*, vol. 41, pp. 2177–2186, 1995.
24. A. D. Gosman, Developments in Industrial Computational Fluid Dynamics, *Trans. IChemE. A*, vol. 76, pp. 153–161, 1998.
25. Y.-Y. Tsui and Y.-F. Pan, A Pressure-Correction Method for Incompressible Flow Using Unstructured Meshes, *Numer. Heat Transfer B*, vol. 49, pp. 43–65, 2006.
26. Y.-Y. Tsui and S.-P. Jung, Analysis of the Flow in Grooved Pumps with Specified Pressure Boundary Conditions, *Vacuum*, vol. 81, pp. 401–410, 2006.
27. V. V. Ranade and J. B. Joshi, Flow Generated by a Disc Turbine: Part 1 Experimental, *Trans. IChemE. A*, vol. 68, pp. 19–33, 1990.